(Received 30 September 2025, Accepted 13 November 2025, Scheduled 23 November 2025)

New Super-Twisting Fast Integral Terminal Sliding Mode Control for PMSM Considering System Aggregate Disturbances

Junqin Liu[1,*], Tianle Li[1], Zhentong Wang[1], Lin Liu[1], Feng Deng[1], Xinchun Jiang[2], Kaihui Zhao[2], Xiangfei Li[2], and Shiyin Gong[3]

[1] *College of Electrical and Information Engineering, Changsha University of Science and Technology, Changsha, Hunan 410114, China*
[2] *College of Transportation and Electrical Engineering, Hunan University of Technology, Zhuzhou 412007, China*
[3] *Hunan Vocational College of Railway Technology, Zhuzhou 412000, China*

ABSTRACT: To effectively suppress parameter perturbations external disturbances and ensure the stability of the PMSM system under uncertain conditions, this paper proposes a novel fast integral terminal sliding mode composite controller (NFITSMC) for speed-loop of PMSM based on super-twisting integral terminal sliding mode disturbance observer (STITSMO). Firstly, the mathematical model of the PMSM with parameter perturbations and external disturbances is analyzed. Then, the NFITSMC speed-loop controller is designed, where the NFIT sliding mode surface combines proportional, integral, and nonlinear terms, enabling effective suppression of parameter perturbations and external disturbances to ensure system stability under uncertainties. Meanwhile, the adaptive exponential switching reaching law adjusts the convergence speed according to the distance between the system state and the sliding surface, thereby mitigating system chattering. Next, the STITSMO disturbance observer is designed, in which the IT sliding mode surface is combined with a second-order super-twisting control law, allowing dynamic gain adjustment based on error magnitude to achieve global fast convergence of the adaptive nonlinear system. Finally, simulations and experiments validate that the NFITSMC-STITSMO composite controller demonstrates superior performance in finite-time convergence, robustness, chattering suppression, and disturbance rejection, making it suitable for high-performance and high-order PMSM control systems.

1. INTRODUCTION

Permanent Magnet Synchronous Motor (PMSM), as a key drive device in modern industrial applications, has gained wide adoption due to its compact structure, precise control, and high operational reliability [1]. PMSMs are extensively utilized in fields with stringent motion control requirements, such as electric vehicle drive systems, high-precision numerical control machining, medical imaging equipment, precision instruments, and aerospace engineering [2]. In recent years, with the continuous development and refinement of advanced control theories such as Direct Torque Control (DTC) [3, 4] and Vector Control [5], PMSM systems have achieved remarkable improvements in speed regulation range, control accuracy, and operational stability. Although vector control technology can provide excellent steady-state performance, the inherent integral saturation problem of the traditional proportional-integral (PI) control strategy [6] limits its effectiveness in handling uncertainties such as parameter variations and external disturbances, making it difficult to meet the stringent requirements of modern high-precision PMSM control systems [7]. It is particularly noteworthy that, in practical operating environments, factors such as temperature variations induce complex disturbances including nonlinear friction and parameter perturbations [8]. These uncertainties not only affect the steady-state characteristics of stator current and electromagnetic torque but also significantly reduce the motion accuracy and smoothness of the controlled system due to torque ripple on the motor shaft, ultimately leading to a decline in the overall efficiency of PMSM traction systems [9].

When a PMSM drives a flexible load, unknown disturbances such as sudden load torque variations, parameter uncertainties, and unmodeled dynamics can degrade control performance and even cause irreversible physical damage to the system. To address this issue, [10] proposed an improved Nonsingular Terminal Sliding Mode Control (INTSMC) algorithm based on a Finite-Time Extended State Observer (FTESO). The FTESO was designed to estimate system disturbances, and its output was used to compensate the INTSMC controller, thereby achieving finite-time convergence and enhancing system robustness. However, considering the insufficient convergence speed of conventional PMSM speed-loop controllers under complex operating conditions, [11] developed a novel Nonsingular Fast Terminal Sliding Mode Control (NNFTSMC) algorithm combined with a Super-Twisting Sliding Mode Observer (STSMO) to improve the dynamic performance of PMSMs. The proposed NNFTSMC works collaboratively with the STSMO, enabling stable control of PMSM drive systems under challenging scenarios such as parameter variations and load disturbances. Similarly, to further enhance the control performance of SPMSMs under complex conditions and improve system fault tolerance, [12] introduced an Improved

* Corresponding author: Junqin Liu (ljq2321925777@163.com).

Model-Free Nonsingular Fast Terminal Sliding Mode Control (IMFNTSMC) algorithm. This approach incorporated a novel ultra-local model, together with a variable-exponent reaching law and a Nonsingular Fast Terminal Sliding Mode (NFTSM) surface, to design a speed-loop IMFNTSMC controller capable of accelerating convergence and effectively suppressing chattering. Moreover, to reduce energy consumption and harmonics in PMSM drive systems, [13] proposed, building on [12], a high-order square-root Cubature Kalman Filter (CKF) with an adaptive estimator, achieving real-time high-precision observation of motor speed and rotor position.

In summary, to accelerate the response speed of the PMSM control system while meeting higher precision control requirements, this paper proposes a composite control algorithm for PMSM, namely the NFITSMC-STITSMO approach. In this scheme, the NFIT sliding mode surface integrates proportional, integral, and nonlinear terms, effectively suppressing parameter perturbations and external disturbances to ensure system stability under uncertain conditions. Meanwhile, the adaptive exponential reaching law adjusts the convergence rate adaptively according to the distance between the system state and the sliding surface, thereby suppressing system chattering. Furthermore, in STITSMO, the integral terminal sliding surface is combined with a second-order super-twisting control law, which enables dynamic gain adjustment based on the error magnitude, achieving global fast convergence for adaptive nonlinear systems. Finally, both simulations and experiments verify that the NFITSMC-STITSMO composite controller demonstrates superior performance in finite-time convergence, robustness, chattering suppression, and disturbance rejection, making it suitable for high-performance and advanced PMSM control system.

2. MATHEMATICAL MODEL OF PMSM

In the absence of disturbance, the mathematical equation of the PMSM in the d-q axis [14] is as follows:

$$\begin{cases} u_d = R_s i_d + L_d \dfrac{di_d}{dt} - L_q \omega_e i_q \\ u_q = R_s i_q + L_q \dfrac{di_q}{dt} + L_d \omega_e i_d + \omega_e \psi_f \\ T_e = \dfrac{3}{2} p_n \left[\psi_f i_q + (L_d - L_q) i_d i_q\right] \\ T_e - T_L = \dfrac{J}{p_n} \dfrac{d\omega_e}{dt} + \dfrac{B}{p_n} \omega_e \end{cases} \tag{1}$$

where u_d denotes the d-axis stator voltage; u_q denotes the q-axis stator voltage; i_d denotes the d-axis stator current; i_q denotes the q-axis stator current; L_d denotes the d-axis inductance; L_q denotes the q-axis stator inductance; R_s denotes the stator resistance; ψ_f denotes the rotor permanent magnet flux linkage; ω_e denotes the electrical angular velocity; T_e denotes the electromagnetic torque; p_n denotes the number of pole pairs; T_L denotes the load torque; J denotes the moment of inertia; and B denotes the damping coefficient.

However, in practical engineering applications, due to factors such as temperature and mechanical stress, PMSM inevitably undergoes parameter perturbations [14]. Eq. (1) can be rewritten as:

$$\begin{cases} u_d = R_s i_d + \dfrac{d\psi_d}{dt} - \omega_e \psi_q + \Delta u_d \\ u_q = R_s i_q + \dfrac{d\psi_q}{dt} + \omega_e \psi_d + \Delta u_q \\ T_e = \dfrac{3}{2} n_p \left[\psi_f + (L_d - L_q) i_d\right] i_q + \Delta T_e \\ \dot{\omega}_e = \dfrac{n_p}{J} \left(T_e - T_L - B\omega_m\right) + \Delta P_n \end{cases} \tag{2}$$

where ω_m represents the mechanical angular velocity; Δu_d, Δu_q represent the disturbance terms caused by variations in R_s, L_d, L_q, and ψ_f; ΔP_n represents the disturbance term caused by variations in the moment of inertia and viscous friction coefficient; and ΔT_e represents the unknown disturbance of the load torque.

Substituting Eq. (2) into Eq. (1) yields:

$$\begin{aligned} \dot{\omega}_e &= \frac{3n_p^2}{2J} \psi_e i_q - \frac{B}{J} \omega_e + \frac{n_p}{J} (\Delta T_e - T_L + \Delta T_L) + \Delta P_n + \delta_d \\ &= \tau_1 i_q + \tau_2 \omega_e + F \end{aligned} \tag{3}$$

where ΔT_L denotes the unknown disturbance of the load torque, while δ_d represents the 'unmodeled dynamics' in the system, including sensor measurement errors, frictional damping, cogging torque, etc.

3. DESIGN OF THE SPEED-LOOP NFITSMC CONTROLLER

3.1. Theoretical Derivation of the NFITSMC Controller

Equation (3) can be simplified as $\dot{\omega}_e = \tau_1 i_q + \tau_2 \omega_e + F$. Letting the error between the reference angular velocity and the actual angular velocity of the motor be chosen as the state variable, i.e., $e_1 = \omega_e^* - \omega_e$, $x_2 = \dot{x}_1 = e_1$. To enhance the robustness of the PMSM system and improve tracking performance, a novel fast integral terminal sliding mode controller (NFITSMC) [15] is proposed:

$$s = x_2 + \mu_1 x_1 + \int_{t_0}^{t} \left(\mu_2 |x_1|^{\lambda_1} \operatorname{sgn}(x_1) + \mu_3 |x_2|^{\lambda_2} \operatorname{sgn}(x_2)\right) dt \tag{4}$$

where μ_1, μ_2, μ_3, λ_1, and λ_2 are positive constants to be designed, subject to the conditions $0 < \lambda_1 < 1$ and $\lambda_2 = \frac{2\lambda_1}{1+\lambda_1}$.

In Eq. (4), the introduced terminal term enables the system to reach equilibrium in finite time. Differentiating (4) yields:

$$\dot{s} = \dot{x}_2 + \mu_1 x_2 + \mu_2 |x_1|^{\lambda_1} \operatorname{sgn}(x_1) + \mu_3 |x_2|^{\lambda_2} \operatorname{sgn}(x_2) \tag{5}$$

To achieve a balance between convergence speed and chattering, the following adaptive exponential switching reaching law [6] is adopted:

$$\dot{s} = -\left[\frac{-k_a |e_1|}{\lambda + (1-\lambda) e^{-a|s|}} + k_b |s|^{a_1}\right] \operatorname{sgn}(s) - \eta_2 s$$

$$= -\eta_1 \text{sgn}(s) - \eta_2 s \tag{6}$$

where $0 < \lambda < 1$; k_a, k_b, a, a_1, and η_2 are all positive constants to be designed.

To ensure that the state variables remain on the sliding surface, by setting $\dot{s} = 0$ in Eq. (5) and Eq. (6), the equivalent control laws u_e and u_s can be obtained as:

$$\begin{cases} u_e = \dfrac{1}{\tau_1}\begin{pmatrix} \dot{\omega}_e^* - \tau_2\omega_e - \hat{F} + \mu_1 x_2 + \\ \mu_2 \left|x_1\right|^{\lambda_1} \text{sgn}\left(x_1\right) + \mu_3 \left|x_2\right|^{\lambda_2} \text{sgn}\left(x_2\right) \end{pmatrix} \\ u_s = \dfrac{1}{\tau_1}\left(\eta_1 \text{sgn}(s) + \eta_2 s\right) \end{cases} \tag{7}$$

According to Eq. (7), the output i_q^* of the speed-loop controller is given by:

$$i_q^* = u_e + u_s \tag{8}$$

3.2. Stability Proof of the NFITSMC Controller

Proof: Selecting the Lyapunov function $V = \frac{1}{2}s^2$ and by differentiating V, we obtain:

$$\begin{aligned} \dot{V} &= s\dot{s} \\ &= s\begin{pmatrix} \dot{\omega}_e^* - \tau_1 u_q - \tau_2\omega_e - F + \mu_1 x_2 \\ +\mu_2 \left|x_1\right|^{\lambda_1} \text{sgn}(x_1) + \mu_3 \left|x_2\right|^{\lambda_2} \text{sgn}(x_2) \end{pmatrix} \\ &= s\begin{bmatrix} \dot{\omega}_e^* - \tau_1\left(u_e + u_s\right) - \tau_2\omega_e - F \\ +\mu_1 x_2 + \mu_2 \left|x_1\right|^{\lambda_1} \text{sgn}(x_1) + \mu_3 \left|x_2\right|^{\lambda_2} \text{sgn}(x_2) \end{bmatrix} \\ &= s\left(-\eta_1 \text{sgn}(s) - \eta_2 s - \tilde{F}\right) \\ &= -\eta_1 \left|s\right| - \eta_2 s^2 - s\left\|\tilde{F}\right\| \le 0 \end{aligned} \tag{9}$$

where $\tilde{F} = \hat{F} - F$ represents the disturbance observation error, which is a bounded quantity; if the observation of the unknown disturbance is sufficiently accurate, then $\tilde{F} = 0$.

According to Lyapunov's stability theorem and LaSalle's invariance principle, the state variable $e_1 = \omega_e^* - \omega_e$ will converge to zero along the sliding surface s within a finite time, which is faster than linear sliding mode (asymptotic convergence) [16].

4. DESIGN OF THE STITSMO DISTURBANCES OBSERVER

4.1. Theoretical Derivation of the STITSMO

To design the super-twisting integral terminal sliding mode disturbance observer, and $\dot{\hat{F}} = \kappa(t)$, $\hat{F} = Au_\chi$:

$$\dot{\hat{\omega}}_e = \tau_1 i_q + \tau_2\hat{\omega}_e + u_\chi + \hat{F} \tag{10}$$

where $\hat{\omega}_e$ denotes the estimated rotor speed; $\hat{F}$ denotes the real-time estimate of the unknown part of the system; u_χ denotes the sliding mode control function to be designed; $A > 0$ denotes the observer gain; and $\kappa(t)$ is a rate of change of F.

By combining Eq. (10) and Eq. (3), and defining $x = \hat{\omega}_e - \omega_e$ and $\tilde{F} = \hat{F} - F$, the error equation is obtained as

$$\dot{x} = \tau_2 x + \tilde{F} + u_\chi \tag{11}$$

where $\dot{\tilde{F}} = Au_\chi - \kappa(t)$.

Super-twisting sliding mode control law can effectively mitigate the chattering problem inherent in conventional sliding mode control and enhance the system's disturbance rejection capability. Its main feature is that the switching function can be hidden through integration, which works similarly to a low-pass filter by converting discontinuous signals into continuous ones. This effectively reduces the adverse effects of the high gain introduced by the switching function on the system. Defining $s_1 = x$, the second-order super-twisting control law [17] is selected as follows:

$$\dot{s}_1 = -r_1 \left|x\right|^{\frac{1}{2}} \text{sgn}\left(x\right) + \xi + \tilde{F} \tag{12}$$

where $\xi = -\int r_2 \text{sgn}\left(x\right)dt$; r_1 and r_2 are positive constants to be designed.

The integral terminal sliding surface [18] is adopted as:

$$s_2 = x + \nu\int_{t_0}^{t} \left|x\right|^k \text{sgn}(x)dt \tag{13}$$

where ν is a parameter to be designed, subject to the conditions $\nu > 0$ and $0 < k < 1$.

Differentiating Eq. (13) yields:

$$\dot{s}_2 = \dot{x} + \nu \left|x\right|^k \text{sgn}(x) \tag{14}$$

It follows from Eq. (12) and Eq. (14) that the control law of the observer is given by:

$$u_\chi = u_1 + u_2 \tag{15}$$

where $u_1 = -\tau_2 x$; $u_2 = -\nu \left|x\right|^k \text{sgn}(x) - r_1 \left|x\right|^{\frac{1}{2}} \text{sgn}\left(x\right) - r_2 \text{sgn}\left(x\right)$.

4.2. Stability Proof of the STITSMO

Proof 1: Selecting the Lyapunov function

$$V_1 = \frac{1}{2}x^2 \tag{16}$$

Differentiating it yields:

$$\begin{aligned} \dot{V}_1 &= x\dot{x} \\ &= x\left(-\nu \left|x\right|^k \text{sgn}(x)\right) \le 0 \end{aligned} \tag{17}$$

According to Lyapunov's stability theorem, the origin is globally stable [19]. By setting $\dot{s}_1 = 0$ in Eq. (14):

$$\dot{x} = -\nu \left|x\right|^k \text{sgn}(x) \tag{18}$$

By performing a differential transformation on Eq. (18) and solving, one obtains:

$$\int_{x_0}^{0} x^{-k}dx = \int_{0}^{T} -\nu dt \tag{19}$$

Calculating the left-hand side of Eq. (19) yields:

$$\int_{x_0}^{0} x^{-k}dx = \left[\frac{x^{1-k}}{1-k}\right]_{x_0}^{0} = -\frac{x_0^{1-k}}{1-k} \tag{20}$$

Similarly, calculating the right-hand side of Eq. (19) yields:

$$\int_{0}^{T} -vdt = -vT \tag{21}$$

From Eq. (20) and Eq. (21), it can be seen that

$$T = \frac{x_0^{1-k}}{v\,(1-k)} \leq \frac{|x_0|^{1-k}}{v\,(1-k)} \tag{22}$$

Therefore, the state error will converge within a finite time T, and the system remains stable.

Proof 2: Selecting a quasi-quadratic positive definite Lyapunov function as follows [20]:

$$V_1(x) = 2r_2|x| + \frac{1}{2}\xi^2 + \frac{1}{2}\left(r_1|x|^{\frac{1}{2}}\operatorname{sgn}(x) - \xi\right)^2 \tag{23}$$

Equation (23) can be simplified as:

$$V_1 = \boldsymbol{\sigma}^T\mathbf{Y}\sigma \tag{24}$$

where $\boldsymbol{\sigma} = \begin{bmatrix} |x|^{\frac{1}{2}}\operatorname{sgn}(x) \\ \xi \end{bmatrix}$; $\mathbf{Y} = \frac{1}{2}\begin{pmatrix} 4r_2 + r_1^2 & -r_1 \\ -r_1 & 2 \end{pmatrix}$.

If $r_1 > 0$, $r_2 > 0$. Then, V_1 is a positive definite continuous matrix.

Differentiating $\boldsymbol{\sigma}$ first gives:

$$\begin{aligned}\dot{\boldsymbol{\sigma}} &= \frac{1}{|x|^{\frac{1}{2}}}\left[\begin{bmatrix} -\frac{1}{2}r_1 & \frac{1}{2} \\ -r_2 & 0 \end{bmatrix}\boldsymbol{\sigma} + \begin{bmatrix} \frac{\tilde{F}}{2} \\ 0 \end{bmatrix}\right] \\ &= \frac{1}{|x|^{\frac{1}{2}}}(\mathbf{B}\boldsymbol{\sigma} + \boldsymbol{\eta})\end{aligned} \tag{25}$$

Differentiating $V_1(x)$ yields:

$$\begin{aligned}\dot{V}_1 &= \frac{1}{|x|^{\frac{1}{2}}}\left[\sigma^T\mathbf{B}^T\mathbf{Y}\sigma + \boldsymbol{\eta}^T\mathbf{Y}\sigma\right] + \frac{1}{|x|^{\frac{1}{2}}}\left[\boldsymbol{\sigma}^T\mathbf{Y}\mathbf{B}\sigma + \boldsymbol{\sigma}^T\mathbf{Y}\eta\right] \\ &\leq -\frac{1}{|x|^{\frac{1}{2}}}\boldsymbol{\sigma}^T\mathbf{X}\zeta + \vartheta\mathbf{q}_1^T\boldsymbol{\sigma}\end{aligned} \tag{26}$$

where $\mathbf{q}_1^T = \begin{bmatrix} \left(2r_2 + \frac{r_1^2}{2}\right) & -\frac{r_1}{2} \end{bmatrix}$; $\mathbf{X} = \frac{r_1}{2}\begin{bmatrix} 2r_2 + r_1^2 & -r_1 \\ -r_1 & 1 \end{bmatrix}$; $\tilde{F} \leq \vartheta|x|^{\frac{1}{2}}$.

The range of $\vartheta\mathbf{q}_1^T\boldsymbol{\sigma}$ is:

$$\vartheta\mathbf{q}_1^T\boldsymbol{\sigma} \leq \frac{1}{|x|^{\frac{1}{2}}}\boldsymbol{\sigma}^T\mathbf{N}\sigma \tag{27}$$

where $\mathbf{N} = \frac{r_1}{2}\begin{bmatrix} \left(4\frac{r_2}{r_1} + r_1\right)\vartheta & -\frac{1}{2}\vartheta \\ -\frac{1}{2}\vartheta & 0 \end{bmatrix}$.

By combining Eqs. (26) and (27), one obtains:

$$\dot{V}_1 \leq -\frac{1}{|x|^{\frac{1}{2}}}\boldsymbol{\sigma}^T\mathbf{X}\boldsymbol{\sigma} + \frac{1}{|x|^{\frac{1}{2}}}\boldsymbol{\sigma}^T M\boldsymbol{\sigma} = -\frac{1}{|x|^{\frac{1}{2}}}\boldsymbol{\sigma}^T\left[\tilde{\mathbf{X}}\right]\boldsymbol{\sigma} \tag{28}$$

where $\tilde{\mathbf{X}} = \frac{r_1}{2}\begin{bmatrix} 2r_2 + r_1^2 - \left(\frac{4r_2}{r_1} + r_1\right)\vartheta & -r_1 + \frac{1}{2}\vartheta \\ -r_1 + \frac{1}{2}\vartheta & 1 \end{bmatrix}$.

From Eq. (28), Eq. (29) can be expressed as:

$$\begin{cases} 2r_2r_1 + r_1^3 - \left(4r_2 + r_1^2\right)\vartheta > 0 \\ \left[2r_2 + r_1^2 - \left(\frac{4r_2}{r_1} + r_1\right)\vartheta\right] > \left(-r_1 + \frac{1}{2}\vartheta\right)^2 \end{cases} \tag{29}$$

From Eq. (29), one obtains:

$$\begin{cases} r_1 > \dfrac{\left(4r_2 + r_1^2\right)\vartheta}{\left(2r_2 + r_1^2\right)} \\ r_2 > \dfrac{16r_2\vartheta + r_1\vartheta^2}{8r_1} \end{cases} \tag{30}$$

If the ranges of parameters r_1 and r_2 satisfy the equation, then $\tilde{\mathbf{X}}$ can be made positive definite.

$$\begin{aligned}\dot{V}_1 &\leq -\frac{1}{|s|^{\frac{1}{2}}}\boldsymbol{\sigma}^T\tilde{\mathbf{X}} \\ &\leq -\frac{1}{|s|^{\frac{1}{2}}}\lambda_{\min}\left\{\tilde{\mathbf{X}}\right\}\|\boldsymbol{\sigma}\|_2^2 \leq -\gamma V_1^{\frac{1}{2}} \leq 0\end{aligned} \tag{31}$$

From Eq. (31), it can be concluded that the state error converges to zero in finite time, ensuring system stability [21].

From Eqs. (11) and (15), $\hat{F}$ can be obtained as:

$$\hat{F} = A\int(u_1 + u_2)dt \tag{32}$$

Throughout the paper, $T(s)$ is used in place of $\operatorname{sgn}(s)$. Compared with the sign function $\operatorname{sgn}(s)$, the switching process of the saturation function $T(s)$ is smoother, thereby mitigating chattering [22].

$$T(s) = \frac{s}{|s| + \varsigma} \tag{33}$$

where $\varsigma > 0$.

5. ANALYSIS OF SIMULATION RESUILS

To verify the effectiveness of the control algorithm proposed in this paper, a simulation model was built in MATLAB, and the proposed algorithm was compared with the PI and FITSMC-STSMO approach. The nominal parameters of the PMSM used in the simulations are listed in Table 1. For the simulation

TABLE 1. The parameters of PMSM.

Motor parameters	Value
Permanent magnet flux linkage ψ_f/Wb	0.171
Stator inductance L_s/ H	0.00334
Stator resistance R_s/Ω	1.9
Number of pole pairs n_p/pairs	4
Moment of inertia J/kg · m^2	0.001469
Damping coefficient B/N · m · s/rad	0.001

TABLE 2. The control parameters of PI/ FITSMC+STSMO/ NFITSMC-STITSMO.

PI	FITSMC+STSMO	NFITSMC-STITSMO
$K_p = 10$	$a_1 = 1050$	$\mu_1 = 1000$
$K_I = 200$	$a_2 = 160$	$\mu_2 = 210$
/	$l_1 = 0.5$	$\mu_3 = 300$
/	$k_1 = 0.66$	$l_1 = 0.5$
/	$k_2 = 0.024$	$\lambda_1 = 0.5$
/	$m_1 = 2000$	$\eta_2 = 0.034$
/	$m_2 = 1050$	$r_1 = 5000$
/	/	$r_2 = 2000$

settings, a fixed-step ode3 (Bogacki-Shampine) solver was selected, the DC bus voltage set to 350 V, and the system sampling frequency was 10 kHz (corresponding to a sampling period of 10 µs). The total simulation time was 1.5 s. Fig. 1 shows the overall control block diagram of the PMSM. Table 2 shows the control parameters of three algorithms.

Remark 1: $\tau_1 = 3n_p^2\psi_e/2J$ and $\tau_2 = -B/J$. The PI parameters are tuned through a sequential approach: first, the current loop is compensated as a Type-I system, and then, with the current loop modeled as an equivalent component, the speed loop is tuned as a typical Type-II system. In the FITSMC+STSMO algorithm, the sliding mode surface is $s = x_2 + a_1x_1 + \int_{t_0}^{t} a_2 |x_1|^{l_1} \operatorname{sgn}(x_1)dt$; the exponential convergence law is $\dot{s} = -k_1\operatorname{sgn}(s) - k_2 s$; and the STSMO is designed to estimate the total system perturbation in real time, $\dot{s} = -m_1 |s|^{\frac{1}{2}} \operatorname{sgn}(s_1) - \int m_2 \operatorname{sgn}(s_1) + F, m_1 > 0, m_2 > 0$.

Remark 2: To better reflect the actual operating conditions of the PMSM, perturbations are introduced into the moment of inertia J and damping coefficient B. The perturbation conditions are applied to the motor parameters, including d-q axis inductances, resistance R_s, moment of inertia$J$, damping coefficient B, and flux linkage ψ_f.

Remark 3: The experimental conditions are set as follows: 1. The speed n changes from 0 r/min to 1000 r/min at 0 s, from 1000 r/min to 2000 r/min at 0.1 s, and from 2000 r/min back to 1000 r/min at 0.3 s; 2. At 0.4 s, ψ_f changes from 0.171 Wb to 0.150 Wb. 3. At 0.5 s, R_s changes from 1.9 Ω to 3.0 Ω. 4. At 0.6 s, L_s changes from 3.34 mH to 4.67 mH. 5. At 0.8 s, J changes from 0.001469 kg·m^2 to 0.002 kg·m^2. 6. At 1.0 s, B changes from 0.001 N · m · s/rad to 0.004 N · m · s/rad. 7. At 1.2 s, T_L changes from 0 N · mto 5N · m.

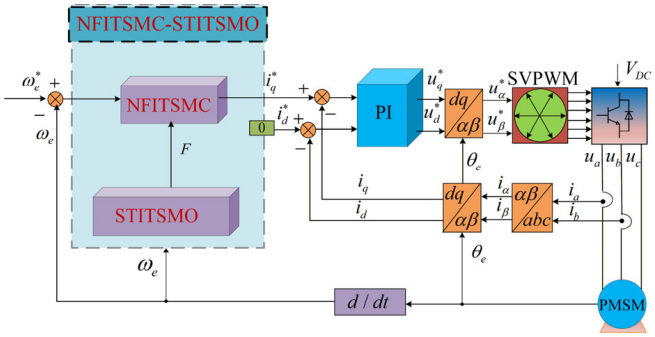

FIGURE 1. Block diagram of the PMSM control system.

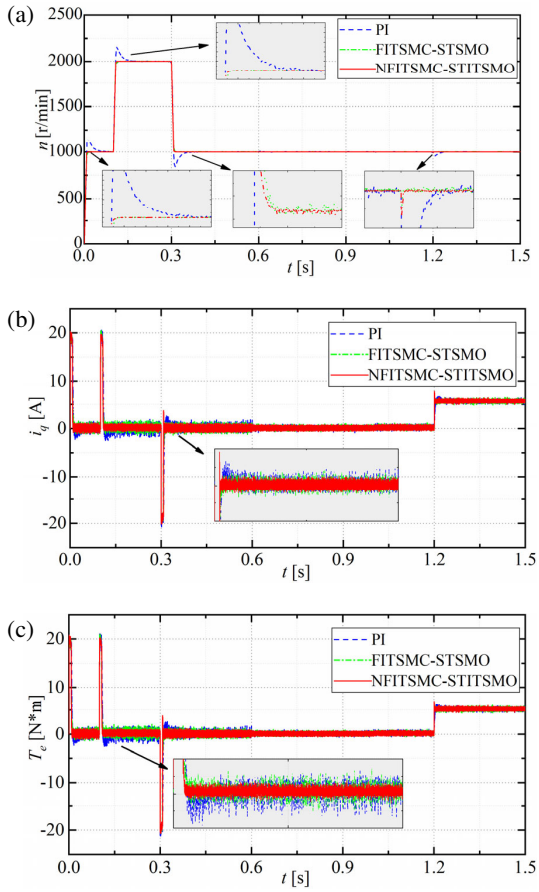

FIGURE 2. Comparative simulation results of speed, current, and torque for three algorithms. (a) Speed of three algorithms. (b) q-axis current of three algorithms. (c) torque of three algorithms.

Figure 2 shows the simulation comparison results of speed, q-axis current, and torque under the three control strategies. From the speed response curve, it can be observed that after the motor starts, during the acceleration phase, the PI control and FITSMC-STSMO method require 0.095 s and 0.015 s, respectively, to reach the reference speed, with the PI controller exhibiting a significant overshoot. In contrast, the proposed NFITSMC-STITSMO method reaches steady state within only 0.01 s, demonstrating the fastest response. When the speed command is stepped from 1000 r/min to 2000 r/min at 0.1 s, the PI method and FITSMC-STSMO method take 0.185 s and 0.117 s, respectively, to track the target speed. By

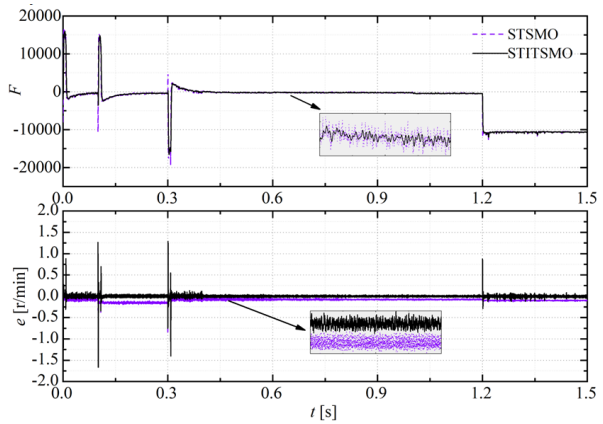

FIGURE 3. Simulation comparison of disturbance observers.

comparison, the NFITSMC-STITSMO strategy reaches the reference speed in 0.108 s, showing superior dynamic response performance. Subsequently, when the speed command decreases from 2000 r/min to 1000 r/min at 0.3 s, the PI control and FITSMC-STSMO control restore steady state at 0.4 s and 0.319 s, respectively, whereas the NFITSMC-STITSMO strategy again exhibits better convergence performance, stabilizing at the target speed as early as 0.312 s. Particularly, under sudden load torque disturbances, both the PI and FITSMC-STSMO controllers show large speed fluctuations and longer settling times, while the proposed method demonstrates stronger robustness and superior dynamic adjustment capability.

In summary, as can be clearly observed from the locally enlarged view in Fig. 2, the proposed control strategy exhibits significant advantages in speed response compared with PI control and FITSMC-STSMO method: it not only achieves smaller steady-state error and faster speed tracking, but also demonstrates stronger robustness against external disturbances and parameter variations. In contrast, the conventional PI and FITSMC-STSMO methods show noticeable speed fluctuations and overshoot during the dynamic process, whereas the proposed method effectively suppresses these unfavorable responses, further improving the control accuracy and operational stability of the system.

From the current and torque simulation curves in Fig. 2, it can be observed that when parameters such as the motor inductance L_s, resistance R_s, and flux linkage ψ_f are perturbed, the FITSMC-STSMO control strategy demonstrates better stability in the output torque and q-axis current waveforms, exhibiting superior control performance under both transient and steady-state conditions. When the moment of inertia is changed at 0.8 s and the damping coefficient at 1.0 s, both PI control and conventional FITSMC-STSMO algorithm show current waveform distortion and increased ripple. In contrast, after a load torque disturbance is applied at 1.2 s, the proposed NFITSMC-STITSMO method achieves the smallest ripples in torque and q-axis current. As can be clearly seen from the locally enlarged plots, the q-axis current and torque ripples under the NFITSMC-STITSMO algorithm are much smaller than those of the PI and FITSMC-STSMO methods, indicating its superior performance in terms of current and torque steady-state quality.

Figure 3 shows the comparison between the traditional STSMO disturbance observer and the proposed STITSMO disturbance observer in terms of system speed tracking error. As can be seen from Fig. 3, STITSMO exhibits superior tracking performance. The locally enlarged view further illustrates that, when motor parameter perturbations occur, the overall tracking error of STITSMO is smaller, converges rapidly to the vicinity of zero, and the chattering phenomenon during steady-state operation is significantly reduced. Fig. 3 presents the comparison of the observation curves of the total system disturbance F for the two observers. The results indicate that the observation output of STITSMO is smoother, with significantly less chattering than the traditional STSMO. Since the accuracy of the observer directly affects the performance of the controller, STITSMO can quickly respond to motor load variations and parameter perturbations, accurately estimate unknown system disturbances, and thereby effectively enhance the overall control accuracy and robustness of the system.

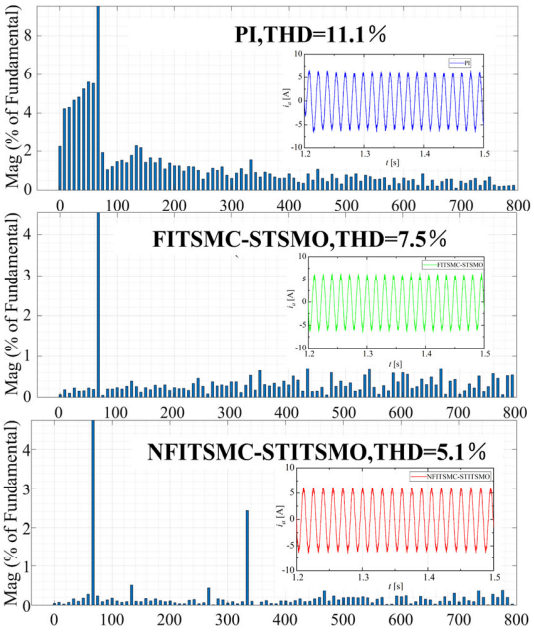

FIGURE 4. The THD analysis of phase-A stator current under three algorithms.

Figure 4 presents the total harmonic distortion (THD) analysis results of the phase-A stator current under the three control methods at rated load conditions. From the harmonic spectrum, it can be observed that the THD value of PI control is 11.1%, with a significant number of harmonic components in the current, leading to poor waveform quality. The FITSMC-STSMO algorithm, by employing an STSMO observer to estimate and compensate for disturbances, improves system robustness and reduces the THD to 7.5%. In contrast, the proposed NFITSMC-STITSMO method, with its designed STITSMO observer, is capable of more accurately estimating system states and suppressing disturbances, further reducing the THD to 5.1%. These results demonstrate that the proposed method exhibits significant advantages in reducing harmonic content, suppressing current ripple caused by parameter perturbations, and improving current quality.

TABLE 3. The comparison of the results for PI, FITSMC-STSMO, and NFITSMC-STITSMO.

Performances	PI	FITSMC-STSMO	NFITSMC-STITSMO
Speed Response	0.12 s	0.03 s	0.017 s
Torque Ripple	15.1%	11.2%	7.34%
THD	11.1%	7.5%	5.1%
Speed Error	54 r/min	9 r/min	3 r/min

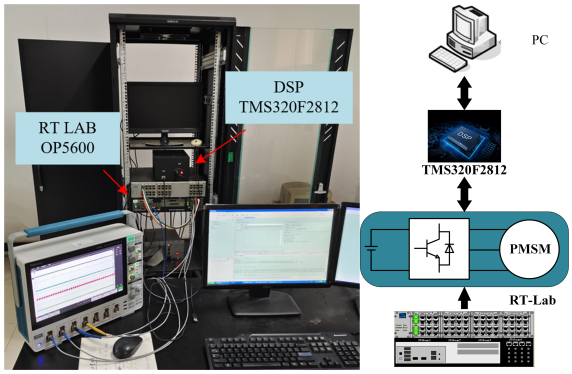

FIGURE 5. The experimental platform of RT-LAB.

6. ANALYSIS OF EXPERIMENTAL RESUILS

To fully verify the practical feasibility of the proposed control method, hardware-in-the-loop (HIL) simulation experiments were carried out on an RT-LAB platform. The experimental system structure is shown in Fig. 5, where the controller is implemented using a TMS320F2812 DSP, and the PMSM drive part is constructed through an OP5600 real-time simulator. All experimental conditions are kept consistent with the aforementioned simulation settings. Fig. 6 presents the comparative experimental waveforms of speed, torque, and q-axis current under parameter perturbations of the motor. The motor and controller parameters used in the experiments are consistent with those in the simulations.

From the hardware-in-the-loop experimental results shown in Fig. 6, it can be observed that the response trends of the three control algorithms are consistent with the simulation results in Fig. 2, further validating the reliability of the simulation model. Under external disturbances and parameter perturbations, both the PI control and FITSMC-STSMO strategy exhibit significant torque and current ripples, with the overall control performance being considerably affected. In contrast, the proposed NFITSMC-STITSMO method is less influenced by uncertainties, demonstrating superior robustness, stability, dynamic performance, and disturbance rejection capability when coping with parameter variations. This performance improvement is mainly attributed to the designed STITSMO observer, which can more accurately estimate the total system disturbance F and provide timely feedforward compensation. As a result, the system's dynamic response speed is significantly improved; current and torque ripples are effectively suppressed; and the overall accuracy and disturbance rejection ability of the motor control system are enhanced. Table 3 summarizes

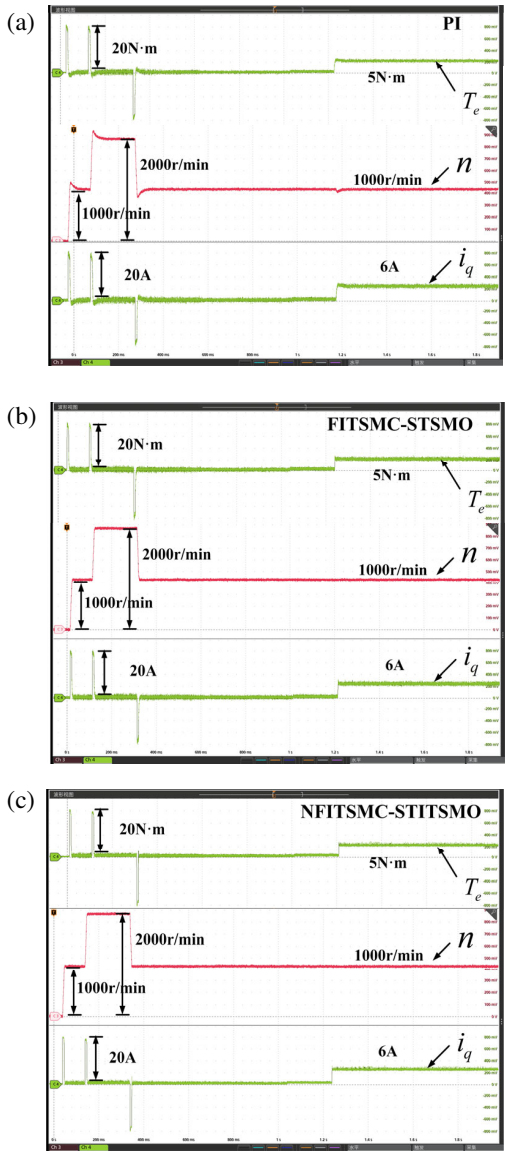

FIGURE 6. Comparison of RT-LAB experimental results. (a) Torque-speed — q-axis current of PI. (b) Torque-speed — q-axis current of FITSMC-STSMO. (c) Torque-speed — q-axis current of NFITSMC-STITSMO.

the performance comparison among PI, FITSMC-STSMO, and NFITSMC-STITSMO.

The comprehensive data presented in Table 3 validate the superior performance of the proposed control method. It is characterized by its capability to achieve fast and overshoot-free speed tracking, deliver smoother speed output, effectively sup-

press transient inrush current, and significantly reduce torque ripple. Collectively, these attributes contribute to enhanced overall operational reliability and control quality of the PMSM drive system.

7. CONCLUSION

To ensure high-precision control performance of the PMSM control system, this paper proposes a composite control algorithm based on NFITSMC and STITSMO. Through comparative simulations and experiments with PI control and conventional FITSMC-STSMO method, the following conclusions are drawn:

i) The NFITSMC controller integrates the advantages of proportional, integral, and nonlinear terms, effectively suppressing parameter perturbations and external disturbances to ensure system stability under uncertain conditions. Combined with the adaptive exponential switching reaching law, it adaptively adjusts the convergence speed according to the distance between the system state and sliding surface, thereby suppressing system chattering.

ii) In STITSMO, integral terminal sliding mode (ITSM) surface together with the second-order super-twisting control law allows dynamic gain adjustment based on the error magnitude, achieving global fast convergence for adaptive nonlinear systems.

iii) Both simulated and experimental results verify that the composite controller enables flexible parameter design, adapts to different system dynamics, and balances convergence speed and robustness. It achieves finite-time convergence and demonstrates superior robustness, chattering suppression, and disturbance rejection capability.

ACKNOWLEDGEMENT

This work was supported by Postgraduate Scientific Research Innovation Project of Hunan Province Grant CX20231107.

REFERENCES

[1] Zhang, Y., P. Yang, C. Liu, S. Li, K. Cao, Z. Liu, and Z. Cheng, "Improved model predictive torque control for PMSM based on anti-stagnation particle swarm online parameter identification," *Progress In Electromagnetics Research B*, Vol. 114, 51–66, 2025.

[2] Zhang, Y., C. Liu, S. Li, K. Cao, Y. Yang, and Z. Cheng, "No weighting factor PMSM model predictive torque control based on composite sliding mode disturbance observer," *Progress In Electromagnetics Research B*, Vol. 113, 63–76, 2025.

[3] Han, L., S. Wang, Z. Wang, X. Zhu, and W. Nie, "Design of compensated PLL for position sensorless drives of PMSMs," *Progress In Electromagnetics Research C*, Vol. 149, 25–35, 2024.

[4] Nan, Y., L. Wang, M. Qi, and Z. Li, "Design of variable boundary layer sliding mode observer for permanent magnet synchronous motor based on fuzzy control," *Progress In Electromagnetics Research C*, Vol. 154, 119–129, 2025.

[5] Li, X., J. Liu, Y. Yin, and K. Zhao, "Improved super-twisting non-singular fast terminal sliding mode control of interior permanent magnet synchronous motor considering time-varying disturbance of the system," *IEEE Access*, Vol. 11, 17 485–17 496, 2023.

[6] Li, X., J. Liu, J. Wang, K. Zhao, Y. Yin, and L. Zou, "Sliding mode control for permanent magnet synchronous motor of sensor-less considering time-varying disturbance," *Electric Drive for Locomotives*, No. 1, 86–96, 2023.

[7] Li, X. F., J. Q. Liu, Y. Yin, *et al.*, "A sensorless sliding mode ADRC for PMSM with time varying disturbances," *Modular Machine Tool & Automatic Manufacturing Technique*, No. 8, 78–83, 2023.

[8] Gong, S. Y., D. Li, J. Q. Liu, *et al.*, "Improved model-free sliding mode control of super-twisting for PMSM," *Modular Machine Tool & Automatic Manufacturing Technique*, No. 2, 175–181, 2024 (in Chinese).

[9] Liu, J., Y. Yang, X. Li, K. Zhao, Z. Yi, and Z. Xin, "Improved model-free continuous super-twisting non-singular fast terminal sliding mode control of IPMSM," *IEEE Access*, Vol. 11, 85 361–85 373, 2023.

[10] He, Y., K. Zhao, Z. Yi, and Y. Huang, "Improved terminal sliding mode control of PMSM dual-inertia system with acceleration feedback based on finite-time ESO," *Progress In Electromagnetics Research M*, Vol. 134, 21–30, 2025.

[11] Wang, J., R. Zhou, and J. Liu, "New non-singular fast terminal sliding mode control of permanent magnet synchronous motor based on super-twisting sliding mode observer," *Progress In Electromagnetics Research C*, Vol. 146, 151–162, 2024.

[12] Li, X., J. Liu, K. Zhao, Y. Yin, and L. Zou, "An improved model-free sliding mode control algorithm of super-twisting for SPMSM," *Progress In Electromagnetics Research C*, Vol. 135, 195–210, 2023.

[13] Li, X., J. Liu, K. Zhao, Y. Yin, and L. Zou, "Improved non-singular fast terminal sensor-less sliding mode control of IPMSM considering external disturbance and parameter perturbation," *Progress In Electromagnetics Research B*, Vol. 102, 81–98, 2023.

[14] Liu, J., Z. Wang, F. Deng, K. Zhao, and X. Li, "Continuous high-order sliding mode optimization control of PMSM based on STSMO," *Progress In Electromagnetics Research Letters*, Vol. 127, 29–37, 2025.

[15] Zhao, K., W. Liu, R. Zhou, W. Dai, S. Wu, P. Qiu, Y. Yin, N. Jia, J. Yi, and G. Huang, "Model-free fast integral terminal sliding-mode control method based on improved fast terminal sliding-mode observer for PMSM with unknown disturbances," *ISA Transactions*, Vol. 143, 572–581, 2023.

[16] Zhao, K. H., L. X. Tu, Y. S. He, *et al.*, "Model-free adaptive fast terminal sliding mode control for PMSM based on compact-form dynamic linearization," *Power System Protection and Control*, 1–12, Aug. 2025 (in Chinese).

[17] Zhao, K., J. Yi, W. Liu, *et al.*, "A model-free super-twisting fast terminal sliding mode control method for a permanent magnet synchronous motor," *Power System Protection and Control*, Vol. 51, No. 22, 88–98, 2023 (in Chinese).

[18] He, Y. S., K. H. Zhao, L. X. Tu, *et al.*, "Model-free terminal sliding mode control for PMSM two-inertia system based on improved ESMDO," *Control Engineering of China*, 1–10, early access, Nov. 2025 (in Chinese).

[19] Jia, N., K. Zhao, Y. Lv, and X. Li, "Non-singular fast terminal sliding mode control torsional vibration suppression for PM synchronous transmission system of EVs," *Progress In Electromagnetics Research M*, Vol. 122, 63–72, 2023.

[20] Li, X. F., Z. X. Yi, J. Q. Liu, *et al.*, "Deep flux weakening of IPMSM based on feedback super-twisting non-singular fast terminal sliding mode control," *Journal of Electronic Measurement and Instrumentation*, Vol. 38, No. 11, 132–145, 2024.

[21] Guo, X., S. Huang, K. Lu, Y. Peng, H. Wang, and J. Yang, "A fast sliding mode speed controller for PMSM based on new compound reaching law with improved sliding mode observer," *IEEE Transactions on Transportation Electrification*, Vol. 9, No. 2, 2955–2968, 2023.

[22] Li, X., Y. Yin, Y. Zhou, W. Liu, and K. Zhao, "The non-singular fast terminal sliding mode control of interior permanent magnet synchronous motor based on deep flux weakening switching point tracking," *Energy Engineering*, Vol. 120, No. 2, 277–297, 2023.